## Supporting Information (JBC online supplement)

# EXPERIMENTAL PROCEDURES

**Reagents.** Unless otherwise noted, all physiological solutions were prepared using sodium phosphate-buffered saline (PBS; 10 mM, pH 7.4) in ultrapure water (Millipore Q). Medical grade air (21% oxygen), nitrogen (0.01% oxygen) and other gas mixtures with defined oxygen concentrations (balance nitrogen) were used without further purification as supplied by Middlesex Gases or Matheson Tri-Gas, Inc. Myxothiazole and potassium cyanide (KCN) were obtained from Fluka Riedel-de-Haën, and 1H-[1,2,4]oxadiazolo[4,2-alpha]quinoxalin-1-one (ODQ) was from Cayman. All other chemicals, including sodium nitrite ($NaNO_2$), sodium nitrate ($NaNO_3$), N-ethylmaleimide (NEM), EDTA, potassium chloride (KCl), HEPES, mannitol, sucrose, glycerol, dithionite, antimycin A, rotenone, diphenyliodonium chloride (DPI), proadifen, resorufin ethyl ether (ethoxyresorufin), oxypurinol, diethyl ether, postassium ferricyanide ($K_3[Fe(CN)_6]$), NADH, NADPH, and DTPA, were obtained at highest available grade from Sigma-Aldrich. Xanthine oxidoreductase (XOR) from either cow milk or buttermilk was obtained from Roche Applied Science and Calbiochem.

**Liver Homogenate Preparation**. Animals were euthanized as described previously after an overnight fast to reduce hepatic lipid and glycogen stores. The liver was rapidly perfused free of blood following cannulation of the hepatic artery and portal vein. Blood-free liver tissue was extirpated into 5 volumes (1:5 w/v) of chilled isotonic liver homogenizing medium (LHM) [containing HEPES (10 mM), mannitol (0.2 M), sucrose (50 mM), KCl (10 mM), and DTPA (50 μM), at pH 7.4] and minced into ~25 $mm^3$ pieces. The mince was gently homogenized (6-7 strokes) using a motor-driven, chilled Potter-Elvehjem glass-Teflon homogenizer to preserve cell membranes and membranous organelles such as mitochondria.

**Cytochrome $P_{450}$ spectrometry.** The P3 microsomal fraction was resuspended in LHM and again subjected to ultracentrifugation (105,000 *g*, 60 min) to minimize carryover of cytosolic constituents. The final pellet was re-suspended in storage buffer [KCl (150 mM), HEPES (10 mM), EDTA (0.1 mM), and glycerol (20%), pH 7.6] and kept at -80°C until use. The Cyt $P_{450}$ content of this (re-centrifuged) microsomal fraction was determined using a dual-beam UV-Vis spectrophotometer (UV-3000, Shimadzu) following reduction with dithionite and equilibration with CO gas. Cytochromes were reduced adding NADPH (1 mM) prior to introducing $NaNO_2$ (100 $\mu$M). Incubations with $NO_2^-$ were carried out in a total volume of 2.5 mL using gas-tight quartz cuvettes containing 2 mg/mL microsomal protein (corresponding to a $P_{450}$ content of 3.1 $\mu$M) at 25°C and pH 7.4 with gentle stirring. Formation of $P_{450}$ intermediates was monitored spectroscopically with successive scans between 390 and 510 nm over 20-25 min.

NO formation by microsomal suspensions incubated with $NaNO_2$ was quantified by headspace analysis using a custom-designed water-jacketed, septum-sealed glass reaction chamber (total volume, 1 mL). Incubations were carried out at 37°C with stirring, and the NO formed in solution was purged and eluted by passing a nitrogen stream over the headspace of the microsomal suspension and quantified in a chemiluminescence NO analyzer. By minimizing foaming and protein denaturation,

this experimental arrangement facilitated NO quantification in the protein-rich sample. Since ferrous nitrosyl complexes are oxygen- and temperature-sensitive, their preservation was enhanced by performing all incubations and manipulations under argon at ambient temperature (22°C).

## RESULTS

**Microsomal Cytochrome $P_{450}$ Mediates Hypoxia-induced $NO_2^-$ Reduction to NO.** Given that the majority of total hepatic $NO_2^-$ reductase activity under hypoxia is in the microsomal fraction, the potential role of the microsomal Cyt $P_{450}$ enzyme system in $NO_2^-$ reduction to NO was investigated. Similar to whole-liver homogenate, NO formation by rat-liver microsomes (P3) depended upon the $NO_2^-$ concentration and was inhibited by oxygen (data not shown). Potential formation of a Cyt $P_{450}$ iron-nitrosyl complex was assessed spectroscopically, and NO formation was independently measured from the head-space of microsomal incubates (Fig. 6*D*). Spectral changes following $NO_2^-$ addition to hypoxic microsomes were evident as increased absorbance in the 440-450 nm region, suggestive of a ferrous nitrosyl complex [Cyt $P_{450}$-$Fe^{II}$(NO)], with a concomitant decrease in the absorbance characteristic of the unbound iron center of Cyt $P_{450}$ (410-420nm). This ferrous-nitrosyl complex is thermodynamically unstable and decomposes to liberate NO, as verified by gas-phase chemiluminescence. After an initial lag phase, NO production rates approached steady-state levels within 20-25 min after addition of $NO_2^-$ to the microsomal suspension and were a function of $NO_2^-$ concentration (Fig. 6*D*, *inset*). Addition of $NO_2^-$ did not yield a Cyt $P_{450}$-$Fe^{II}$(NO) (data not shown). Differences in experimental conditions preclude direct comparison between the time courses of Cyt $P_{450}$-$Fe^{II}$(NO) and NO formation. Consistent with the induction of hepatic $P_{450}$ enzymes by barbiturates, formation of both NO and Cyt $P_{450}$-$Fe^{II}$(NO) from $NO_2^-$ was markedly enhanced in microsomes from phenobarbital-treated animals.

**Mathematical Modeling of $NO_2^-$ Reductase Activity.** To rationalize the NO signals obtained with addition of $NO_2^-$ followed by ferricyanide (**Supplementary Fig. 2**), we considered two models of $NO_2^-$ reductase with generalized properties of heme-proteins in either ferric or ferrous forms. The two models are depicted in **Supplementary Fig. 2 (panels *B* and *C*).** The first model (**panel *B***) is applicable to proposed reductases, such as XOR or cytochrome oxidase, which produce free NO from $NO_2^-$ to nitrosylate ferrous heme proteins. The second model **(panel *C***) is a variation of the first whereby the ferrous heme-protein serves both as a $NO_2^-$ reductase and as target of nitrosylation. Both models assume $k_{on}$ and $k_{off}$ values that are representative of for binding/release of NO with ferrous hemeproteins, i.e., $k_{on} = 10^7\ M^{-1}s^{-1}$ and $k_{off} = 10^{-2}\ s^{-1}$. A rate of $10^{-1}\ s^{-1}$ was chosen for $k_{purge}$, which represents the turnover rate for NO from the purge vessel. We assumed that the action of ferricyanide on tissue nitrosylated heme proteins is where the heme is oxidized as soon as NO is released. The ferricyanide reaction rate ($k_{ferricyan}$) was set to a value such that the heme oxidation by ferricyanide was faster than the spontaneous release of NO from the heme ($100\ M^{-1}s^{-1}$ in our case), ensuring the latter is rate-limiting. Finally, the rate of NO production, $k_{reductase}$ and $k_{oxid}$ was adjusted such that the NO purged from the reaction vessel just before addition of ferricyanide reached a level comparable to what we observed for liver homogenates, i.e. 6-7 ppb (**Supplementary Fig. 2, panel *A***).

In agreement with our data, both models predict a gradual rise in the NO signal upon addition of $NO_2^-$ to the homogenates. The dampened rise is due to capture

of NO by hemes, which initially trap more NO than they release. At t = 1000 s, a sudden burst of NO is registered as ferricyanide addition displaces NO from the heme. Both models, however, predict that the amount of NO released (area under the curve) should not exceed the amount captured (area below the maximal level achieved just prior to ferricyanide addition). This feature differs from the one shown in **panel *A***. Rather, our data suggest that the amount of NO-heme complexes exceeds by nearly two orders of magnitude the amount of free NO captured by the sample. This result suggests that NO-heme species were formed by pathways other than capture of free NO, e.g., direct interaction with $NO_2^-$. Another feature derived from our simulations that differs from our experimental results is the steady-state level reached after ferricyanide addition. While our simulations show that steady-state levels reach values at or below those present just prior to addition of ferricyanide, our experimental levels converge to values that are significantly higher. The higher levels seen post-ferricyanide are consistent with our results obtained with ferricyanide pre-treatment, which we find actually enhances the net $NO_2^-$ reductase activity in tissues. These results corroborate our experimental findings that the bioconversion of $NO_2^-$ reduction to NO in the mammalian tissues probed cannot solely be accounted for by a process whereby free NO is produced from a reaction of $NO_2^-$ with a ferrous heme-protein.

**<u>Supplementary Table 1:</u> Inhibitors used to assess the mechanisms of $NO_2^-$ reduction to NO in rat liver homogenate.**

| Inhibitor | Function | Species Sensitivity | Applied Conc. |
|---|---|---|---|
| ODQ | Oxidizes ferrous ($Fe^{II}$) hemes to ferric ($Fe^{III}$) hemes | Hemoproteins | 10 mM |
| NEM | Alkylates free thiols (-SH) | Thiol moieties | 10 mM |
| Rotenone | Inhibits complex I by preventing transfer of reducing equivalents from NADH dehydrogenase | Mitochondrial $e^-$ transport | 10 $\mu$M |
| Antimycin A | Inhibits complex III by blocking ubiquinol-mediated electron transfer required to reduce complex-III cytochromes | Mitochondrial $e^-$ transport | 100 $\mu$M |
| Myxothiazole | Inhibits electron flow through complex III by preventing the reduction of the cytochrome $bc_1$ complex from ubiquinol | Mitochondrial $e^-$ transport | 3 $\mu$M |
| KCN | Inhibits complex IV (cytochrome oxidase) by coordination to heme | Hemoproteins; mitochondrial $e^-$ transport | 1 mM |
| Oxypurinol | Inhibits XOR | XOR | 100 $\mu$M |
| DPI | Inhibits flavin reductase component of XOR and other flavoproteins | XOR; Cyt $P_{450}$ | 100 $\mu$M |
| Proadifen | Inhibits cyt P-450 monooxygenase activity | Cyt $P_{450}$ | 100 $\mu$M |
| Oxygen | Competes for heme coordination; mitochondrial substrate | Hemoproteins; Mitochondrial $e^-$ transport | 0.2-200 $\mu$M |
| Ethoxyresorufin | Inhibitor of the mitochondrial 1A1 isoform of cyt P-450 | Cyt $P_{450}$; Mitochondrial $e^-$ transport (?) | 18 $\mu$M |

**Supplementary Figure 1:**

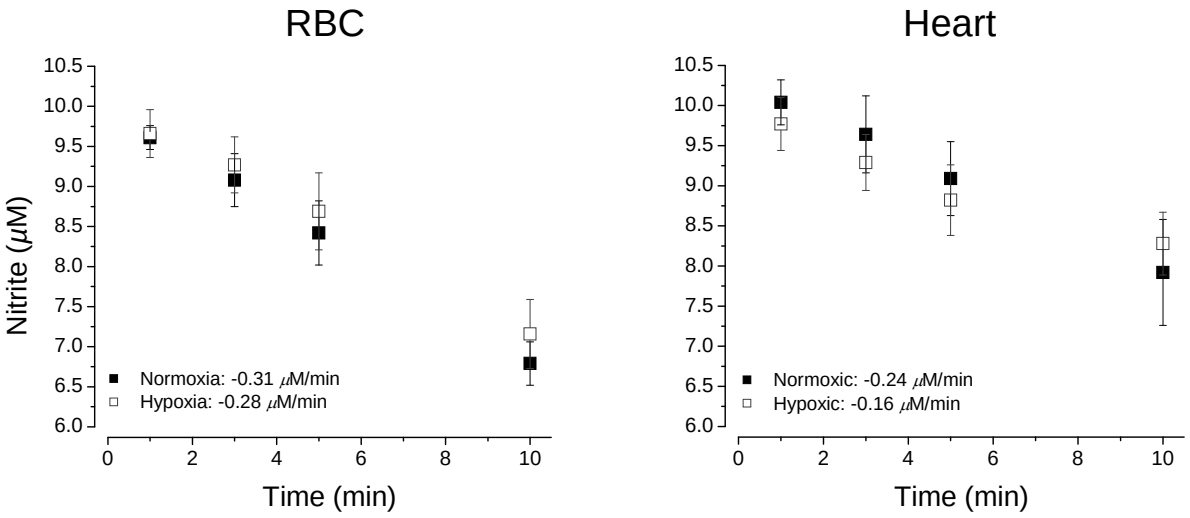


***Suppementary Fig. 1.*** **Nitrite Uptake in RBC and Heart Tissue.** Tissues avidly take up $NO_2^-$ with comparable rates during normoxia and hypoxia.

**Supplementary Figure 2:**

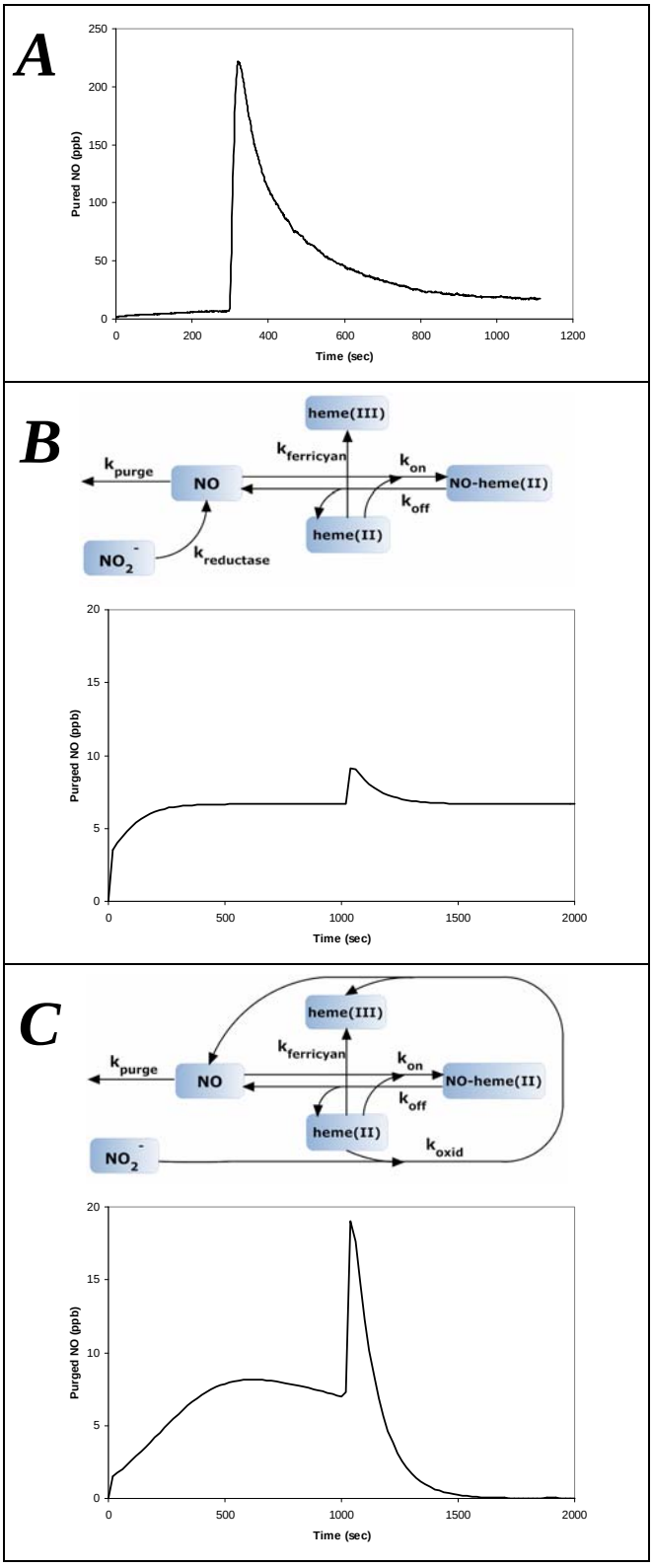

***Suppementary Fig. 2:*** **Mathemical Modeling of Tissue $NO_2^-$ Reductase Activity.** Empirical ferricyanide intervention data derived from experimental studies (panel *A*) contrast with modeled predictions from previously proposed mechanisms leading to tissue NO formation from $NO_2^-$ (panels *B* and *C*). The model depicted in panel *B* assumes the presence of a $NO_2^-$ reductase (e.g., XOR, cytochrome oxidase) that generates free NO from $NO_2^-$, which nitrosylates hemeproteins in the tissues. The model in panel *C* is a variation of *B* whereby the same hemeprotein serves as $NO_2^-$ reductase and as target of nitrosylation. In agreement with our data, both models predict a gradual, but not instantaneous, rise in the signal, due to initial capture of NO by heme, followed by a sudden burst of NO as ferricyanide forces the release of NO from the heme. Both models, however, predict that the amount released should not exceed the amount captured, a feature discordant with our experimental observations. (heme(III) – ferric heme; heme(II) – ferrous heme).